Surface Science 631 (2015) 81–87

Contents lists available at ScienceDirect

Surface Science

journal homepage: www.elsevier.com/locate/susc

Detection of 2D phase transitions at the electrode/electrolyte interface using electrochemical impedance spectroscopy

Jakub Tymoczko [a,b], Viktor Colic [a], Aliaksandr S. Bandarenka [a,*], Wolfgang Schuhmann [a,b,**]

[a] Center for Electrochemical Sciences — CES, Universität Bochum, Universitätsstr. 150, D-44780 Bochum, Germany
[b] Analytische Chemie — Elektroanalytik & Sensorik, Ruhr-Universität Bochum, Universitätsstr. 150, D-44780 Bochum, Germany

ARTICLE INFO

Available online 9 May 2014

Keywords:
Electrochemical impedance spectroscopy
Phase transition
Electrode–electrolyte interface
Constant phase element
Pt(111)
Adsorbate layer

ABSTRACT

The capacitance of the electric double layer, C_{DL}, formed at the electrode/electrolyte interface is generally determined by electrochemical impedance spectroscopy (EIS). However, C_{DL} values obtained using EIS data often depend on the *ac* frequency of the potential perturbation used in EIS. The reasons for the observed frequency dispersions can be various, and hence extracting valuable information about the status of the electrified interface is not possible with the required certainty. In this work, using well-understood electrochemical systems, namely Pt(111) electrodes in contact with a series of acidic sulfate ions containing electrolytes, we provide strong evidence that 2D phase transitions in the adsorbate layers and, in general, structural effects at the electrode/electrolyte interface are in many cases responsible for the frequency dispersion of the double layer capacitance. These empirical findings open new opportunities for the detection and evaluation of 2D phase transition processes and other structural effects using EIS, even in presence of simultaneously occurring electrochemical processes. However, further theoretical elaboration of this effect is necessary.

1. Introduction

Research techniques which use alternating current (*ac*) probing signals are among the most informative non-destructive methods in physical chemistry and electrochemistry. Electrochemical impedance spectroscopy (EIS) is often used as an indispensable tool for in-depth characterisation of the electrode/electrolyte interface [1–5]. EIS allows for the elucidation of physical models of electrochemical systems and for obtaining detailed information about processes taking place simultaneously at electrified interfaces.

Conventional EIS is based on the determination and analysis of two parameters at different *ac* probing frequencies: (*i*) the absolute value of the impedance, $|Z|$, which is the ratio between the amplitudes of the probing *ac* signal (e.g. electrode potential) and the response (e.g. *ac* current), and (*ii*) the phase (time) shift, δ, between the former and the latter. Due to specific properties of electrochemical systems, both $|Z|$ and δ depend on the frequency, ω, of the *ac* signal. The ultimate goal of EIS investigations is to solve the inverse problem [6]: it is necessary to find a suitable *physical* model of the system and to estimate its parameters using the impedance data as a function of the frequency, $|Z|(\omega)$ and $\delta(\omega)$.

According to the classical approach developed by Dolin and Ershler in 1940 [7] and by Randles in 1947 [8], a general EIS model of the electrochemical interface consists of at least three major parts (Fig. 1). The first part is related to the impedance of the electrolyte Z_{el}, which can often be approximated by a resistance if the electrolytes are liquids: $Z_{el} = R_s$. The second part is related to the impedance due to electrochemical processes involving the interfacial charge transfer (Faradaic processes) with the associated impedance Z_F. It should be noted that particular equations describing Z_F depend on many factors, such as the mechanism of the electrochemical reactions, their kinetics or mass transport modes [9]. Finally, the third part of the model is the impedance of the interface itself, Z_i. The response of the latter is normally of capacitive nature. The Dolin–Ershler–Randles approach is to express the model using a formula for the total impedance, Z_{tot}: $Z_{tot} = Z_{el} + (Z_i^{-1} + Z_F^{-1})^{-1}$, which corresponds to a general equivalent circuit as shown in Fig. 1. The parallel combination of Z_F and Z_i reflects the underlying hypothesis that the current due to electrochemical processes can be roughly considered as a "leakage" of the interfacial "capacitor".

Whilst theories describing Z_F for various reactions and mechanisms are relatively well developed [3,10,11], the interpretation of the interfacial impedance (Z_i) is unfortunately not straightforward. The main constraint is that the *ac* perturbation probing the electrode/electrolyte interface reveals that a seemingly capacitive behaviour of the so-called interfacial electric double layer often does not obey the rules of an ideal capacitance and it turns out that the measured capacitance of the double layer depends on the applied *ac* frequency. This empirical fact can be formally described using a so-called constant phase element

* Corresponding author.
** Correspondence to: W. Schuhmann, Center for Electrochemical Sciences — CES, Universität Bochum, Universitätsstr. 150, D-44780 Bochum, Germany.
E-mail addresses: aliaksandr.bandarenka@rub.de (A.S. Bandarenka), wolfgang.schuhmann@rub.de (W. Schuhmann).

http://dx.doi.org/10.1016/j.susc.2014.04.014
0039-6028/

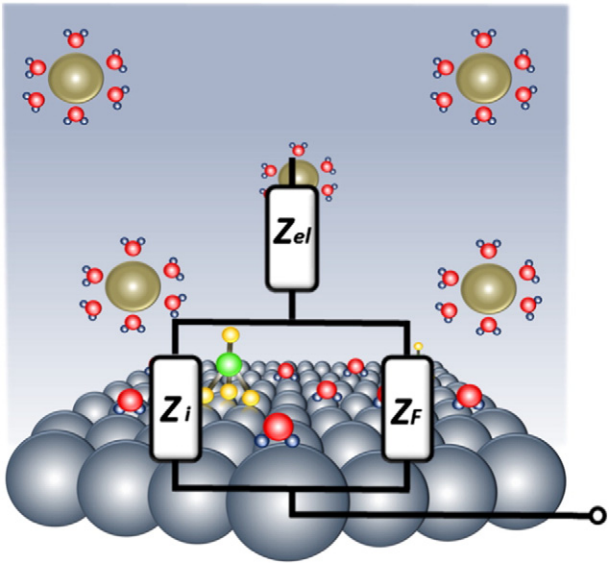

Fig. 1. A generalised physical model (equivalent electric circuit, EEC) describing the electrode/electrolyte interface according to the Dolin–Ershler–Randles approximation. The impedance spectra of electrochemical interfaces contain the response of the ionically conducting electrolyte, Z_{el}, the response of the interface itself, Z_i, and the contributions originating from electrochemical (Faradaic) reactions, Z_F.

(CPE) with a specific formula given as $Z_i = C'^{-1}_{DL}(j\omega)^{-\varphi}$, where C'_{DL} is the parameter, which is proportional to the double layer capacitance, and $\varphi \leq 1$ is the CPE-exponent, which is directly related to the above-mentioned "frequency dispersion". When $\varphi = 1$, the CPE behaviour corresponds to that of an ideal capacitor. Remarkably, responses of numerous systems of different natures can be *formally* represented by a simple exponential formula as presented above [12]. Nevertheless, the above-discussed CPE phenomenon complicates the analysis of EIS data and significantly decreases the informative power of the method itself.

In different periods of the development of EIS, numerous hypotheses and theories were proposed to explain the CPE behaviour of the double layer [9,12–19]. The essential idea of those hypotheses is that the observed non-ideal behaviour is exclusively due to a "chaotic performance" of the double layer caused by one of the following reasons: (*i*) a low concentration of working electrolyte or the presence of contamination [9,19], (*ii*) roughness of electrodes [9,14,15,17], (*iii*) disturbing electrochemical (Faradaic) reactions or non-uniform (or fractal) properties of the electrodes themselves [9,15,17,18], and (*iv*) other specific phenomena and effects which can be classified as measurement "artefacts". Unfortunately, numerous experimental facts suggest that none of these theories can explain the whole variety of experimental observations on this subject. Moreover, some of them even contradict those concepts. Likely, there could be more than one reason for the frequency dispersion in each particular case.

Concerning the response of electrified interfaces between solid electrodes and liquid electrolytes, recent experiments with well-defined single crystal metal electrodes provide evidence that in many cases the CPE-behaviour of the electrochemical interface is not a consequence of its "chaotic performance". On the contrary, it is likely a consequence of structural effects at the boundary between electrodes and electrolytes. Pajkossy [13], Kolb and Pajkossy [20] and Motheo et al. [21] suggested that 2D and 3D structuring effects in the electric double layer caused by adsorbates hinder its ability to respond ideally to the *ac*-probing.

In this manuscript, we extend our previous work on the elucidation of the nature of the *ac*-response of the electrochemical interface [22–24] using one of the most well understood model systems in electrochemical science, namely the interface between Pt(111) electrodes and aqueous sulfuric acid solutions. Specifically, we further test the hypothesis of Pajkossy, Kolb and Motheo et al. by changing important parameters in this system such as the electrolyte concentration, the nature of the electrolyte components and the presence of disturbing Faradaic reactions. Our findings provide probably the best evidence confirming the above-mentioned hypothesis that structural effects at the electrode/electrolyte interface govern the CPE-behaviour during *ac*-probing. These findings open up new opportunities for the detection of 2D phase transitions and other structuring effects using impedance spectroscopy.

2. Experimental

Two Pt(111) crystals (MaTeck, Germany, 5 mm diameter, oriented better than 0.1°, roughness 30 nm) were used to ensure high reproducibility of data. The electrochemical cell for preparation and characterisation of single crystal electrodes was described in detail elsewhere [25]. Pt(111) electrodes were selected instead of Au(111) as the former exhibits much lower surface mobility of Pt atoms at room temperature, simplifying data interpretation. The following chemicals were used to prepare working electrolytes: H_2SO_4 (Merck, Suprapur) and K_2SO_4 (Aldrich, 99.99% trace metal basis).

The EIS measurement scheme was the same as in Ref. [24]. Frequencies between 30 kHz and 1 Hz with 5 mV amplitude of the probing signals were used. Issues related to modelling and fitting of large experimental EIS datasets are reported in detail elsewhere [26]. The quality of the measured impedance spectra was evaluated using the "linear" [27] and "logarithmic" [28] Kramers–Kronig check procedures. The output of the fitting procedure was controlled by the root-mean-square deviations and estimated individual parameter errors using home-made "EIS Data Analysis 1.0" software to ensure the validity of the model and correctness of the fitting, as described in detail elsewhere [29,30].

A mercury–mercury sulfate reference electrode (MMS) was kept in a separate compartment and separated from the working electrolyte with an ionically conducting ceramic insert. A polycrystalline Pt wire was used as counter electrode. All potentials are referred to the RHE scale. A VSP-300 potentiostat (Bio-Logic, France) was used to control the electrochemical measurements. Measurements involving rotating disc electrodes (RDE) were performed using a Pine RDE 710 instrument (USA).

3. Results and discussion

3.1. Cyclic voltammetry and impedance analysis

Fig. 2 shows a cyclic voltammogram typical for Pt(111) single crystal electrodes in contact with 0.05 M H_2SO_4 electrolyte. The voltammogram reveals several processes involving the interfacial charge transfer at different electrode potentials. Broad peaks between 0.05 V and ~0.35 V disclose surface limited adsorption and desorption of hydrogen. The potential region between ~0.35 V and ~0.55 V is attributed to adsorption/desorption of (bi)sulfate anions with a pair of sharp peaks due to order/disorder phase transitions in the (bi)sulfate adsorbate layer to form predominantly a $(\sqrt{3} \times \sqrt{7})R19.1°$ superstructure with co-adsorbed H_2O molecules at the surface with an anion coverage of 0.2 monolayer (ML), as indicated in Fig. 2. It should be noted that the above-mentioned superstructure co-exists with a denser adsorbate structure, namely a (3×1) superstructure with a corresponding (bi)sulfate adsorbate coverage of 1/3 ML [31]. A pair of relatively small peaks in the potential region between approximately 0.7 V and 0.9 V is associated with an order/disorder phase transition, as revealed by electrochemical scanning tunnelling microscopy [31].

In order to explore the potential regions where the order/disorder and disorder/order phase transitions take place, impedance spectra have been recorded between 0.37 V and 0.92 V. In this potential region, the physical model of the interface (expressed in terms of EEC) is

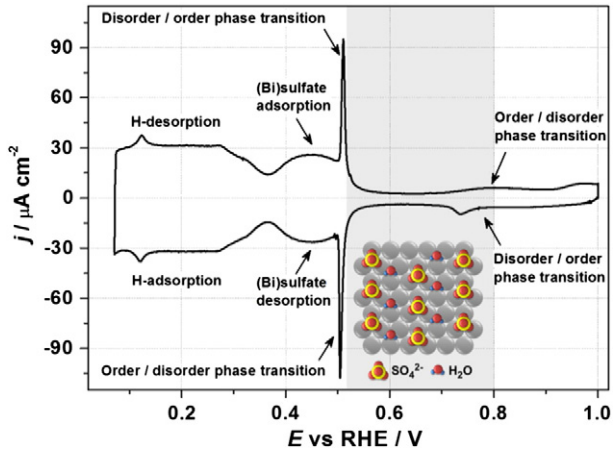

Fig. 2. Typical potentiodynamic cyclic voltammogram ($dE/dt = 50$ mV/s) characterising a Pt(111) single crystal in 0.05 M H_2SO_4. The inset shows the model of the (bi)sulfate adlayer ($\sqrt{3} \times \sqrt{7}$)R19.1° superstructure with co-adsorbed H_2O molecules formed at Pt(111) terraces in contact with H_2SO_4 with its stability region between ~0.53 V and ~0.8 V, as proposed in [31].

relatively simple, as proven previously [22,32–34]. This corresponding model is shown in Fig. 3, where the Faradaic impedance for the (bi)sulfate adsorption/desorption is composed of a series combination of the adsorption resistance, R_{ads}, and capacitance, C_{ads}. A possible contribution of diffusion in the given frequency region is neglected by using a relatively high concentration of SO_4^{2-} in the electrolyte. The interfacial double layer impedance, $Z_i = Z_{dl}$, is modelled by a CPE. The uncompensated (solution) resistance is modelled by the resistance R_s.

Fig. 4 shows several examples of impedance spectra with the corresponding fitting results. The EEC shown in Fig. 3 fits well the experimental data for Pt(111) in contact with a 0.05 M H_2SO_4 with normalized root-mean square deviations of less than 3% in the whole investigated potential region. It should be noted that it also accurately describes the EIS response of Pt(111)-electrodes in contact with other electrolytes used in this work. Therefore, it is possible to identify and separate the response associated with sulfate adsorption and the interfacial double layer itself, by means of electrochemical impedance spectroscopy. Fig. 5 summarises the results of the EIS investigation showing the dependences of the EEC parameters on the electrode potential.

Fig. 5A represents the dependence of the adsorption capacitance, $C_{ads}(E)$, on the electrode potential. It basically correlates with the cyclic voltammogram shown in Fig. 2 in the relevant potential regions. Notably, whilst $C_{ads}(E)$ is associated with adsorption of (bi)sulfates, it is possible to quantify the amount of these anions adsorbed on the

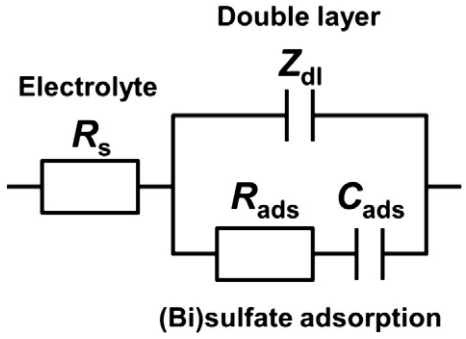

Fig. 3. Physical model (equivalent electric circuit) of the Pt(111)/electrolyte interface in sulfate containing media in the potential region between ~0.35 V and ~1.0 V. R_s — electrolyte resistance, Z_{dl} — impedance of the double layer, C_{ads} — adsorption capacitance, and R_{ads} — adsorption resistance.

electrode surface by integrating the $C_{ads}(E)$ curve assuming a one-electron interfacial transfer. The resulting charge is approximately 55 μC·cm^{-2} corresponding to a (bi)sulfate coverage of approximately 0.23 ML. This coverage is between the values for the co-existing ($\sqrt{3} \times \sqrt{7}$)R19.1° and (3×1) structures.

Fig. 5B shows the corresponding dependence of the inverse adsorption resistance, $R_{ads}^{-1}(E)$, on the potential. As expected [35], $R_{ads}^{-1}(E)$ largely correlates with the $C_{ads}(E)$.

Fig. 5C and D shows the dependencies of the CPE parameters on the electrode potential, namely the parameter which is proportional to the double layer capacitance, $C'_{DL}(E)$, and the corresponding exponent $\varphi(E)$. The former dependence shows peaks in the potential range between 0.37 V and 0.6 V, where it correlates with the $C_{ads}(E)$ and CV, and between 0.7 V and 0.85 V, where a broad current peak is observed in the anodic part of the voltammogram. Those peaks at more anodic potentials likely appear as a result of fast specific adsorption of *OH (where * designates the adsorbed species) and/or possible H_2O rearrangements in the double layer, inducing the order/disorder phase transition. Unfortunately, it is not possible to distinguish this fast adsorption as a separate process using EIS analysis [32].

Fig. 5D shows the dependence of the CPE exponent, $\varphi(E)$. In general, these dependencies show how the energy of the *ac* probing signal in EIS experiments dissipates at different stages of the experiment, linking the fraction of the dissipated energy, $Diss_{CPE}$, in one harmonic cycle and the CPE exponent φ [12]:

$$Diss_{CPE}(\%) = \cos(\varphi\pi/2) \cdot 100\%.$$

Interestingly, in the potential region between 0.37 V and 0.6 V (Fig. 5D), where the most intensive anodic current is detected in the CV (compare Fig. 2) due to sulfate adsorption at Pt(111), the double layer demonstrates almost ideal capacitive behaviour with CPE exponents being very close to 1. There is a pronounced minimum, which is designated with (1) in Fig. 5D at potentials where the disorder/order phase transition occurs, which is in accordance with STM measurements [31]. Interestingly, the CPE exponent values do not rise back to their initial values in the potential region of stable ordered superstructures. It is especially striking as almost no significant Faradaic processes are revealed in the CV (Fig. 2) within this potential region. At the potentials of approximately 0.8 V where the disorder/order phase transition occurs, a well-pronounced peak with a shoulder is seen in the $\varphi(E)$ curve (Fig. 5D) (designated as 2 and 3, respectively). Again, no direct correlation between the absolute values of the current in the cyclic voltammogram can be noticed: CPE-exponent values are much lower as compared with those corresponding to the butterfly peaks in the CV, whilst the absolute values of the voltammetric currents are much smaller. This additionally supports the statement that the CPE-behaviour can hardly be explained by the previously discussed "chaotic performance" concepts. From Fig. 5D, it is evident that peaks in the $\varphi(E)$ dependence correlate well with the 2D phase transitions. On the other hand, whilst the CVs show only one pair of peaks in the potential region between 0.7 V and 0.85 V (Fig. 5D), merged peaks (2) and (3) in the $\varphi(E)$ dependence likely reveal complex restructuring processes at the interface due to additional adsorption of *OH in this potential region.

In the following, we focus only on the dependencies of $\varphi(E)$ and we further explore how they change with changing the important parameters in this system, such as the electrolyte concentration, the nature of the electrolyte components, and the presence of other Faradaic reactions.

3.2. Effect of H_2SO_4 concentration

Fig. 6 shows a series of cyclic voltammograms obtained for Pt(111) in contact with H_2SO_4 electrolytes of different concentrations. The CVs are plotted versus the RHE scale in order to disclose effects which are mainly attributed to the changes in (bi)sulfate concentration. From

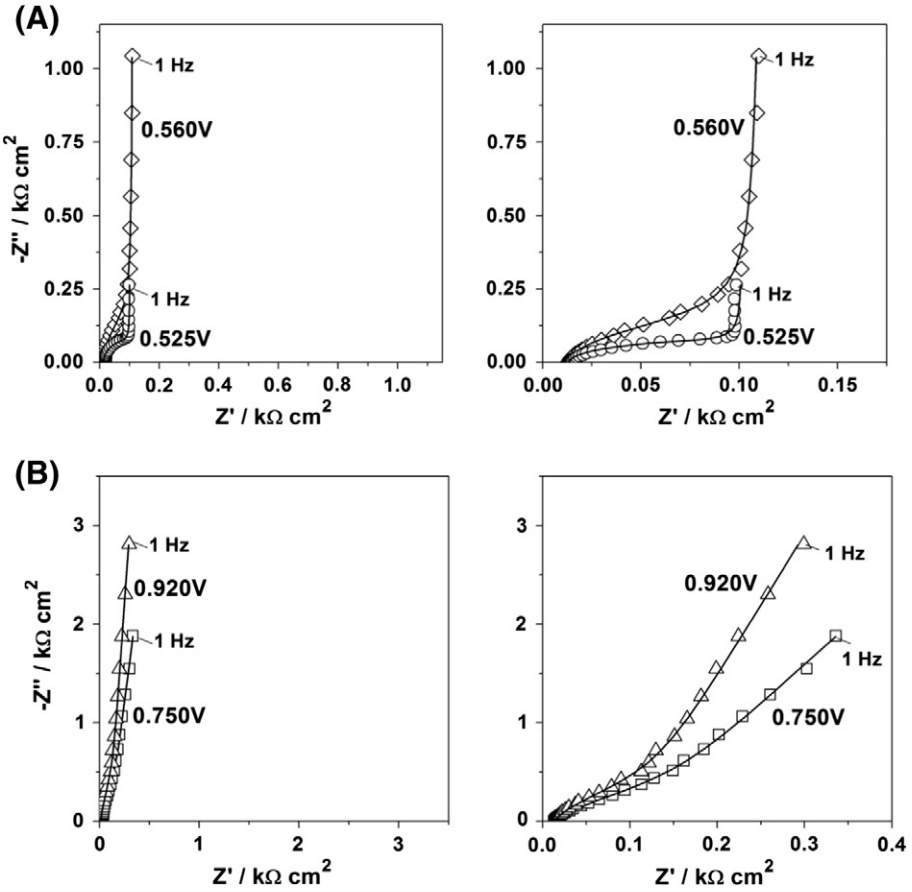

Fig. 4. Examples of Nyquist plots of experimental EIS data (open symbols) together with fitting results (solid lines) for selected electrode potentials. Left and right pictures show the same data using the equidistant scale for the representation of imaginary numbers (left) and using an expanded scale for the x-axes (right).

the figure it is evident that the increase in H_2SO_4 concentration does not significantly affect the hydrogen adsorption/desorption region between 0.05 V and ~0.35 V. In contrast, the peaks attributed to the (bi)sulfate adsorption/desorption as well as the disorder/order and order/disorder phase transitions in the adsorbed (bi)sulfate layer are shifted towards more negative potentials, as indicated in Fig. 6 with arrows. Notably, the shift in the sharp butterfly peaks corresponds well with the behaviour for a one-electron interfacial charge transfer.

The effect of the increased H_2SO_4 concentration on $\varphi(E)$ dependencies is illustrated in Fig. 7. Evidently, with the increase in the electrolyte concentration by almost one order of magnitude it is not possible to "raise" the values of the CPE exponent. This additionally questions the former hypothesis that the CPE-behaviour is more pronounced in diluted electrolytes. Conversely, minima (1–3) become even more prominent and, particularly, the peaks (2–3) become well-separated (Fig. 7). One can observe the same tendency as in the CVs shown in Fig. 6: all the characteristic minima in Fig. 7 are shifted towards more negative potentials. Therefore, one can further confirm that indeed the low constant phase element exponent values are due to structural effects at the electrified interface. This is especially interesting as CVs reveal only one pair of relatively broad peaks, making $\varphi(E)$ dependencies a good complimentary mean to detect more accurately interfacial rearrangements.

We hypothesise that minima (2) in Fig. 7 can be tentatively associated with transitions between co-existing $(\sqrt{3} \times \sqrt{7})$R19.1° and (3×1) structures, as this peak is more affected by the change in the (bi)sulfate concentration compared to peak (3). We attribute the latter peak to the order/disorder interfacial rearrangements. However, further investigations are necessary to clarify the exact origin of these two peaks.

In the following section, based on the assumption that low CPE-exponent values disclose interfacial structural effects, we explore how concurrent Faradaic reactions, particularly the oxygen reduction reaction, influence the $\varphi(E)$ dependencies.

3.3. Effect of concurrent oxygen reduction reaction

Fig. 8A summarises essential information on how the $\varphi(E)$ dependencies for the Pt(111) surface change in the presence of O_2 in 0.05 M H_2SO_4 as compared with the oxygen-free electrolyte. For the purpose of brevity we do not present the whole EIS analysis and all EEC parameter dependencies. To additionally ensure the correctness of the impedance analysis in this particular case and to separate two simultaneously occurring processes, namely the adsorption of (bi)sulfates and the oxygen electroreduction, Fig. 8B compares the extracted inverses of the charge transfer resistance for the ORR, $R_{ORR}^{-1}(E)$, with a relevant RDE-voltammogram. Taking into account that the inverse of the charge transfer resistance is proportional to the current derivative, i_{ORR}, $R_{ORR}^{-1}(E) \approx \partial i_{ORR} / \partial E$, the maximum of the $R_{ORR}^{-1}(E)$ should be close to the pseudo half-wave potential of the RDE-voltammogram. Fig. 8B illustrates that, indeed, this is the case, additionally confirming the correctness of the used fitting procedures. Fig. 8C also presents the EEC used for the fitting, which is also similar to that elucidated previously in refs [23,24].

Fig. 8A demonstrates, that ORR significantly affects $\varphi(E)$ dependencies in the region of structuration in the adsorbed (bi)sulfate anions, in contrast to the Pt(111)/$HClO_4$ interface, where dissolved O_2 changes the whole picture only slightly [23,24]. In the presence of the oxygen

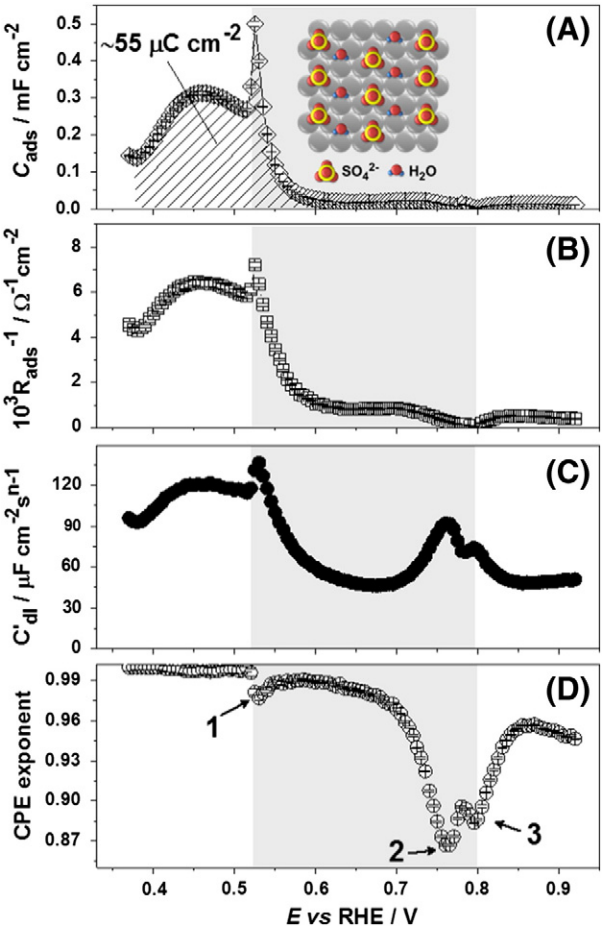

Fig. 5. Parameters of the model shown in Fig. 3 as a function of the electrode potential: (A) (bi)sulfate adsorption capacitance, $C_{ads}(E)$, (B) inverses of the (bi)sulfate adsorption resistance, $R_{ads}^{-1}(E)$, (C) CPE-parameter, which is proportional to the double layer capacitance, $C'_{DL}(E)$, and (D) the corresponding CPE-exponent, φ.

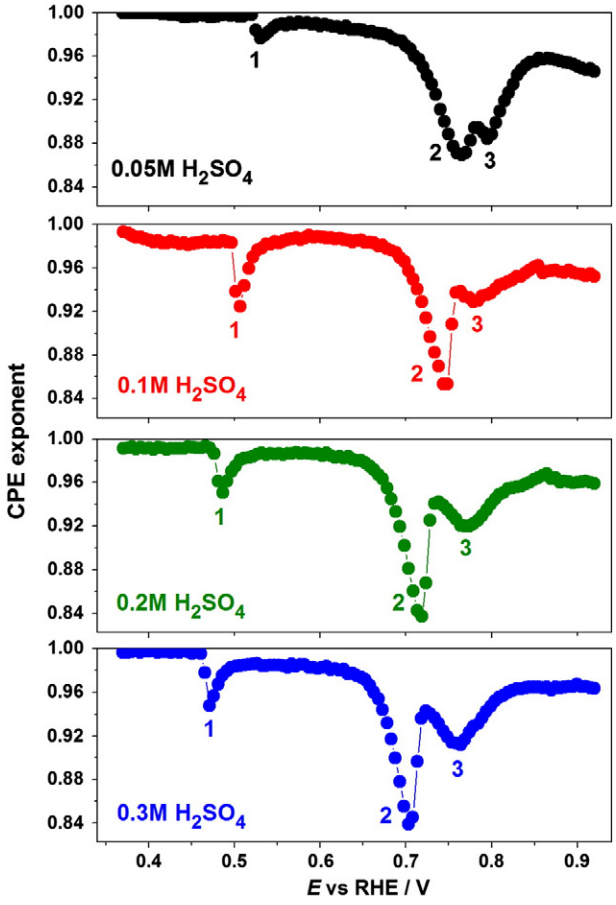

Fig. 7. Dependencies of the CPE exponent, φ, on the electrode potential for Pt(111) in 0.05 M, 0.1 M, 0.2 M, and 0.3 M H_2SO_4.

reduction reaction, the peaks (1–3) of the corresponding $\varphi(E)$ dependence merge. However, Fig. 8A suggests that the ordering in the sulfate adlayer starts at approximately the same potential as compared to the O_2-free 0.05 M H_2SO_4 and the CPE exponent starts decreasing almost synchronously in both cases. Another observation is that $\varphi(E)$ reproducibly increases back to approximately 1 by ~0.8 V, when the cathodic ORR current is still significant. Again, this behaviour confirms that the frequency dispersion does not clearly correlate with Faradaic currents themselves. Therefore, we hypothesise that the potential region of structuration in the sulfate adlayer still exists in the presence of the ORR, though, it is slightly narrower.

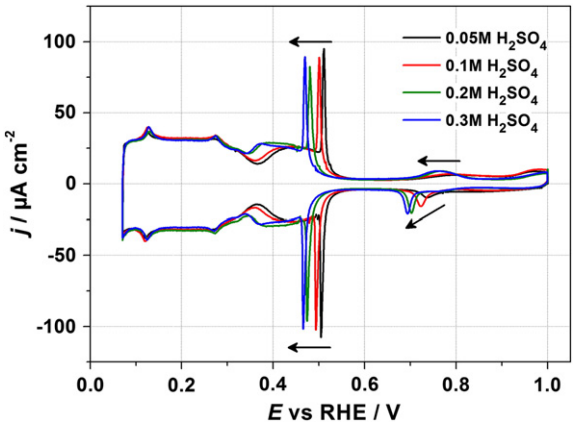

Fig. 6. Typical cyclic voltammograms of Pt(111) in 0.05 M, 0.1 M, 0.2 M, and 0.3 M H_2SO_4. $dE/dt = 50$ mV/s.

3.4. Effect of K^+ addition

The effect of addition of different alkali metal cations on electrochemical response of the Pt(111)/electrolyte interface has been reported earlier [36–38]. Fig. 9 illustrates the effect of K^+ addition on the $\varphi(E)$ dependence in the potential region of (bi)sulfate adsorption. The figure also reveals changes in the related cyclic voltammogram upon addition of 0.05 M K_2SO_4: a pair of sharp peaks appears at approximately 0.7 V (Fig. 9B). At this potentials, an additional poorly resolved minimum appears in the corresponding $\varphi(E)$ dependence (Fig. 9B), suggesting that cations, such as K^+, play an important role in structural rearrangements in the adsorbed layer. Whilst the exact nature of these structural rearrangements might not be entirely clear from EIS measurements, Fig. 9 gives an additional illustrative example of how to use $\varphi(E)$ to detect them with relatively high sensitivity.

4. Concluding remarks

In summary, using a relatively well-understood model system, we have demonstrated that the so-called frequency dispersion of the double layer is largely governed by 2D phase transitions in the adlayers and, in general, by structural effects at the electrode/electrolyte interface. We propose that this result can be used for the detection of 2D phase transitions and other structuring effects using electrochemical

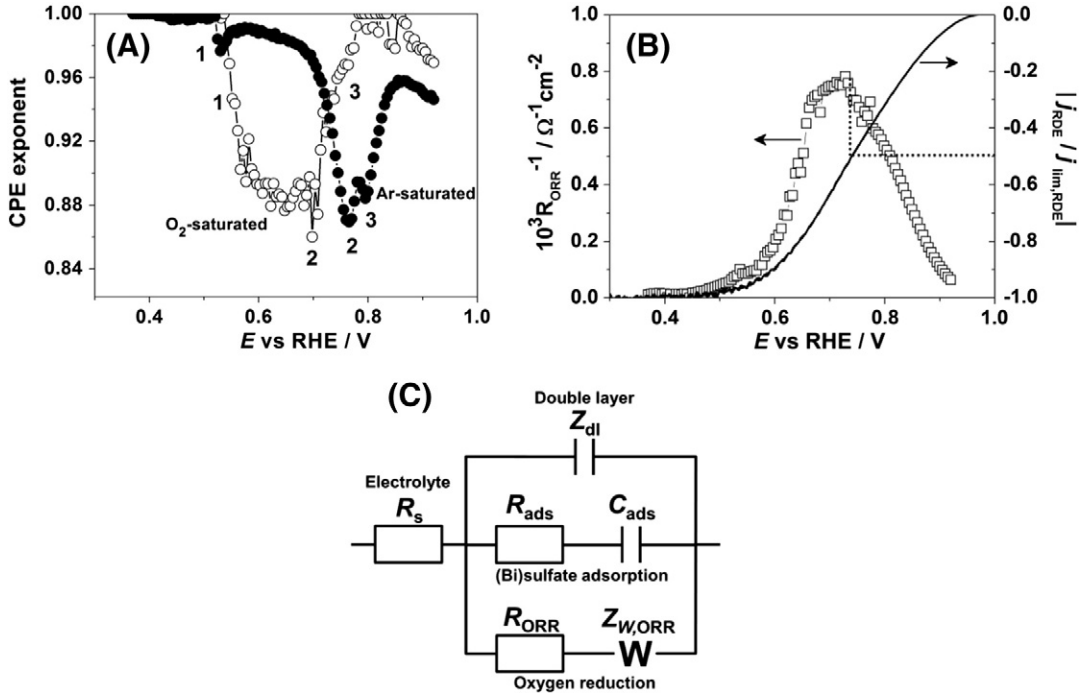

Fig. 8. (A) Dependencies of the CPE exponent on the electrode potential for Pt(111) in Ar-saturated (solid symbols) and O_2-saturated (open symbols) 0.05 M H_2SO_4. (B) also shows the inverses of the charge transfer resistance of the ORR as a function of the electrode potential and the ORR-current recorded in a separate experiment using RDE (1600 rpm, $dE/dt = 50$ mV/s). Dotted lines in (B) demonstrate that the half-wave potential of the current corresponds to the maximum of $R_{ORR}^{-1}(E)$, as expected. (C) also shows the equivalent electric circuit used in the impedance analysis ($Z_{W,ORR}$ denotes the diffusional Warburg impedance).

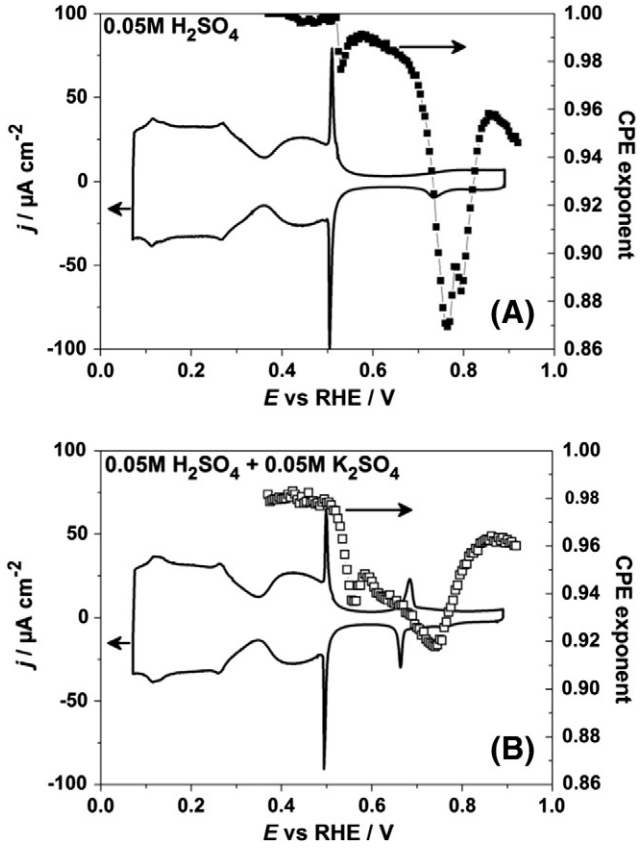

Fig. 9. Typical cyclic voltammograms of Pt(111) in electrolytes containing (A) 0.05 M H_2SO_4 and (B) 0.05 M H_2SO_4 + 0.05 M K_2SO_4, ($dE/dt = 50$ mV/s) together with the corresponding dependencies of the CPE exponent on the potential in the same electrolytes.

impedance spectroscopy. The dependence of the constant phase element exponent on the electrode potential can help in revealing these effects and in monitoring of how they are affected by the electrolyte concentration, by the nature of the electrolyte components and by the presence of disturbing Faradaic reactions. However, further theoretical elaboration of these phenomena is required.

Acknowledgements

Financial support from the Cluster of Excellence RESOLV (EXC 1069) funded by the DFG (Deutsche Forschungsgemeinschaft) and in the framework of Helmholtz-Energie-Allianz "Stationäre elektrochemische Speicher und Wandler" (HA-E-0002) is gratefully acknowledged.

References

[1] D.D. Macdonald, Electrochim. Acta 51 (2006) 1376.
[2] B.-Y. Chang, S.-M. Park, Annu. Rev. Anal. Chem. 3 (2010) 207.
[3] M.E. Orazem, B. Tribollet, Electrochemical Impedance Spectroscopy, John Wiley & Sons, New Jersey, 2008. (560 pp.).
[4] J.B. Jorcin, M.E. Orazem, N. Pebere, B. Tribollet, Electrochim. Acta 51 (2006) 1473–1479.
[5] A.S. Bandarenka, Analyst 138 (2013) 5540.
[6] A. Tarantola, Inverse Problem Theory and Methods for Model Parameter Estimation, 1 ed. Siam, Philadelphia, 2005. (342 pp.).
[7] P.I. Dolin, B.V. Ershler, Acta Physicochem. URSS 13 (1940) 747.
[8] J.E.B. Randles, Discuss. Faraday Soc. 1 (1947) 11.
[9] A. Lasia, in: B.E. Conway, J. Bockris, R.E. White (Eds.), Modern Aspects of Electrochemistry, vol. 32, Kluwer Academic/Plenum Publishers, NY, 1999, p. 143.
[10] X. Wu, H. Ma, S. Chen, Z. Xu, A. Sui, J. Electrochem. Soc. 146 (1999) 1847–1853.
[11] E. Barsoukov, J.R. Macdonald, Impedance Spectroscopy: Theory, Experiment, and Applications, Wiley, New Jersey, 2005. (616 pp.).
[12] A. Sadkowski, A.J. Motheo, R.S. Neves, J. Electroanal. Chem. 455 (1998) 107.
[13] T. Pajkossy, J. Electroanal. Chem. 364 (1994) 111.
[14] Z. Kerner, T. Pajkossy, Electrochim. Acta 46 (2000) 207.
[15] A.E. Larsen, D.G. Grier, T.C. Halsey, Phys. Rev. E. 52 (1995) R2161.
[16] T.I. Borisova, B.V. Ershler, Zh. Fiz. Khim. 25 (1950) 337.
[17] A. Le Mehaute, G. Crepy, Solid State Ionics 9 (10) (1983) 17.
[18] J. Newman, J. Electrochem. Soc. 117 (1970) 198.

[19] M.H. Martin, A. Lasia, Electrochim. Acta 56 (2011) 8058.
[20] T. Pajkossy, D.M. Kolb, Electrochim. Acta 53 (2008) 7403.
[21] A.J. Motheo, A. Sadkowski, R.S. Neves, J. Electroanal. Chem. 430 (1997) 253.
[22] J. Tymoczko, W. Schuhmann, A.S. Bandarenka, Electrochem. Commun. 27 (2013) 425.
[23] A.S. Bondarenko, I.E.L. Stephens, L. Bech, I. Chorkendorff, Electrochim. Acta 82 (2012) 517.
[24] A.S. Bondarenko, I.E.L. Stephens, H.A. Hansen, F.J. Perez-Alonso, V. Tripkovic, T.P. Johansson, J. Rossmeisl, J.K. Nørskov, I. Chorkendorff, Langmuir 27 (2011) 2058.
[25] J. Tymoczko, W. Schuhmann, A.S. Bandarenka, Phys. Chem. Chem. Phys. 15 (2013) 12998, http://dx.doi.org/10.1039/C3CP51998H.
[26] A.S. Bondarenko, Anal. Chim. Acta. 743 (2012) 41.
[27] B. Boukamp, J. Electrochem. Soc. 142 (1995) 1885.
[28] C.A. Schiller, F. Richter, E. Gülzow, N. Wagner, Phys. Chem. Chem. Phys. 3 (2001) 374.
[29] B.B. Berkes, A. Maljusch, W. Schuhmann, A.S. Bondarenko, J. Phys. Chem. C 115 (2011) 9122.
[30] B.B. Berkes, J.B. Henry, M. Huang, A.S. Bondarenko, ChemPhysChem 13 (2012) 3210.
[31] B. Braunschweig, W. Daum, Langmuir 25 (2009) 11112.
[32] B.E. Conway, J. Barber, S. Morin, Electrochim. Acta 44 (1998) 1109.
[33] S. Morin, H. Dumont, B.E. Conway, J. Electroanal. Chem. 412 (1996) 39.
[34] B.B. Berkes, G. Inzelt, W. Schuhmann, A.S. Bondarenko, J. Phys. Chem. C 116 (2012) 10995.
[35] A. Lasia, in: J. O'M. Bokris, B.E. Conway (Eds.), Modern Aspects of Electrochemistry, vol 35, Kluwer Academic/Plenum Publishers, NY, 2002, p. 233.
[36] V. Climent, N. García-Araez, J.M. Feliu, Electrochem. Commun. 8 (2006) 1577.
[37] E. Sibert, R. Faure, R. Durand, J. Electroanal. Chem. 515 (2001) 71.
[38] E. Sibert, R. Faure, R. Durand, J. Electroanal. Chem. 528 (2002) 39.